

# Resolved atomic interaction sidebands in an optical clock transition

M. Bishof<sup>1</sup>, Y. Lin<sup>1</sup>, M. D. Swallows<sup>1</sup>, A. V. Gorshkov<sup>2</sup>, J. Ye<sup>1</sup> and A. M. Rey<sup>1</sup>

<sup>1</sup> *JILA and Department of Physics, NIST and University of Colorado, Boulder, CO 80309-0440, USA and*

<sup>2</sup> *Institute for Quantum Information, California Institute of Technology, Pasadena, CA 91125, USA*

(Dated: March 26, 2022)

We report the observation of resolved atomic interaction sidebands (ISB) in the  $^{87}\text{Sr}$  optical clock transition when atoms at microkelvin temperatures are confined in a two-dimensional (2D) optical lattice. The ISB are a manifestation of the strong interactions that occur between atoms confined in a quasi-one-dimensional geometry and disappear when the confinement is relaxed along one dimension. The emergence of ISB is linked to the recently observed suppression of collisional frequency shifts in [1]. At the current temperatures, the ISB can be resolved but are broad. At lower temperatures, ISB are predicted to be substantially narrower and usable as powerful spectroscopic tools in strongly interacting alkaline-earth gases.

Experimental efforts in control of ultracold alkaline-earth atoms (AEA), such as Sr or Yb, have led to remarkable developments in optical atomic clocks [1, 2], which are approaching the accuracy of single ion standards [3]. Fermionic AEA are also beginning to attract considerable attention in the context of quantum information processing [4] and quantum simulation [5, 6]. Many of these applications require reaching the strongly interacting regime, in which interactions dominate over all relevant dynamical energy scales. In this Letter, we demonstrate the onset of strong interactions in a low dimensional gas of  $^{87}\text{Sr}$  atoms by observing resolved interaction sidebands (ISB) in Rabi spectroscopy of the  $^1S_0 - ^3P_0$  optical clock transition.

Rabi spectroscopy has served as an excellent probe for interacting alkali gases. For example, it was used to detect and characterize Bose Einstein condensation in spin polarized hydrogen [7], to directly measure the fermion pair wave function in the BEC-BCS crossover [8], and to resolve the Mott insulator shell structure in a bosonic lattice system [9]. Here, we show that the ISB structure that emerges during optical Rabi interrogation can become a powerful spectroscopy tool to uniquely probe lattice-trapped AEA. At microkelvin temperatures and loading conditions of mainly one or two atoms per lattice site, we observe a single ISB, which can be resolved from the carrier but is broad. However, in the quantum degenerate regime, the ISB are expected to become substantially narrower and could thus lead to a precise determination of the  $s$ -wave  $^1S_0 - ^3P_0$  interaction parameters (currently, the  $^1S_0 - ^3P_0$  scattering lengths for fermionic AEA remain unknown). In addition, we show that the variation in ISB spectra between sites with different numbers of atoms allows for a precise characterization of atom number occupations in interacting AEA systems.

When the  $^1S_0$  and  $^3P_0$  electronic degrees of freedom within a single fermionic atom are represented as an effective pseudo-spin 1/2 ( $g$  and  $e$ ), two nuclear-spin polarized atoms form a simple model for understanding the appearance of ISB (see Fig. 1). We consider atoms trapped in a tube geometry with a weak trapping frequency  $\omega_Z$  along  $\hat{Z}$  and a strong transverse confinement  $\hbar\omega_{X,Y} \gg k_B T_{X,Y}$ , large enough to forbid any transverse dynamics [ $T_X(T_Y)$  is the temperature along  $\hat{X}(\hat{Y})$ ]. We assume the atoms are initially prepared in

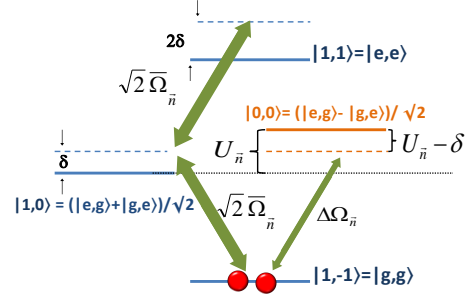


FIG. 1: (Color online) Schematic diagram of Rabi spectroscopy in the strongly interacting regime. When  $\delta \approx 0$ , only the non-interacting triplet states ( $S = 1$ ) are accessible, giving rise to an interaction-free carrier. However, when  $\delta \sim U_{\vec{n}}$ , the singlet  $|0, 0\rangle$  becomes resonant, and a slightly inhomogeneous coupling ( $\Delta\Omega_{\vec{n}} \neq 0$ ) can induce population transfer to it, as manifested in an ISB.

the same pseudo-spin state ( $|gg\rangle$ ) and interrogated by a linearly polarized laser beam with bare Rabi frequency  $\Omega^B$  and detuning from the atomic resonance  $\delta$ . The Pauli exclusion principle forces atoms in identical internal states to occupy different vibrational levels along  $\hat{Z}$ ,  $\vec{n} = (n_1, n_2)$ , since their spatial wave function must be antisymmetric. Being identical fermions, the atoms initially experience zero  $s$ -wave interaction. If the atoms are coherently driven to  $e$  (i.e. if they experience the same Rabi frequency  $\bar{\Omega}_{\vec{n}} \equiv (\Omega_{n_1} + \Omega_{n_2})/2$ ), then the effective spin must remain symmetric under exchange. Consequently, during the excitation the atoms will not experience any  $s$ -wave interactions. We refer to states with spin-symmetric wave functions,  $|gg\rangle \equiv |S = 1, M = -1\rangle$ ,  $|ee\rangle \equiv |1, 1\rangle$  and  $(|eg\rangle + |ge\rangle)/\sqrt{2} \equiv |1, 0\rangle$ , as the triplet states,  $S = 1$  [10, 11].

However, in optical transitions, a small component of the probe beam along  $\hat{Z}$  leads to a slightly different Rabi frequency  $\Omega_{n_j}(\eta_Z^2)$  for each mode, with  $\eta_Z = k_Z a_{ho}^Z/\sqrt{2}$  the Lamb-Dicke parameter,  $m$  the atom mass,  $k_Z$  the component of the probe laser wave vector along  $\hat{Z}$  and  $a_{ho}^Z = \sqrt{\frac{\hbar}{m\omega_Z}}$  the  $\hat{Z}$  harmonic oscillator length. If  $\Delta\Omega_{\vec{n}} = (\Omega_{n_1} - \Omega_{n_2})/\sqrt{2}$  is not zero, then the optical excitation-induced inhomogeneity

can transfer some of the atoms to the antisymmetric pseudo-spin singlet state,  $(|eg\rangle - |ge\rangle)/\sqrt{2} \equiv |0,0\rangle$ . The interacting singlet is separated from  $|1,0\rangle$  by an interaction energy  $U_{\bar{n}}$ .

In the limit where  $\delta \sim \Omega_{\bar{n}} \ll U_{\bar{n}}$ , a small  $\Delta\Omega_{\bar{n}}$  cannot overcome the energy cost required to drive the transition to the singlet (see Fig. 1). Evolution into the singlet is blocked and the atoms remain non-interacting. However, if we increase the detuning to  $\delta \sim U_{\bar{n}}$ , the transition  $|1,-1\rangle \rightarrow |0,0\rangle$  becomes resonant. Here, a small  $\Delta\Omega_{\bar{n}}$  can efficiently transfer the atoms to the singlet, giving rise to an ISB in the lineshape. Note that if instead of preparing all the atoms in  $g$  we prepare the atoms in  $e$ , the ISB occurs at  $\delta \sim -U_{\bar{n}}$ .

The ISB resemble motional sidebands that develop in spectroscopy of trapped ions when the trapping frequency is much larger than the recoil energy, the so called Lamb-Dicke regime [12]. In this case, the carrier becomes free of Doppler shifts up to the corresponding ‘‘Stark shift’’ [13], and all motional effects are manifested in the sidebands. In our case, the ISB are pushed away from the carrier due to the large energy separation between interacting and non-interacting states, leaving the carrier free from interaction effects, up to a correction proportional to  $\Delta\Omega_{\bar{n}}^2/U_{\bar{n}}$ . Recently we have observed the suppression of collisional frequency shifts to the  $10^{-17}$  level under similar tight trapping conditions [1]. The observation of ISB unambiguously confirms this suppression to be the consequence of reaching the strongly interacting regime.

Our experiment employs nuclear spin-polarized ( $m_I = +9/2$ )  $^{87}\text{Sr}$  atoms loaded in two lattice configurations: a one-dimensional (1D) vertical lattice which creates an array of quasi-two-dimensional traps (pancakes) along  $\hat{Y}$  with weak confinement along the  $\hat{X}$  and  $\hat{Z}$  directions, and a deep 2D lattice which creates an array of quasi-1D traps (tubes) in the  $\hat{X}$ - $\hat{Y}$  plane and has weak confinement along  $\hat{Z}$ . To prepare the atomic system, we laser cool  $^{87}\text{Sr}$  atoms to about  $2\ \mu\text{K}$  inside a magneto-optic trap based on the weak  $^1S_0 - ^3P_1$  transition and then load them into a 1D vertical lattice. The spatial distribution of occupied 1D lattice sites is determined by the vertical extent of the MOT cloud, which is approximately Gaussian with a standard deviation  $\sigma_V = 30\ \mu\text{m}$ . For the 2D lattice confinement we then adiabatically ramp up the horizontal lattice (along  $\hat{X}$ ). To remove any atoms trapped in the 1D vertical lattice outside the 2D intersection region, we ramp the vertical lattice off and then back on. The number of horizontal lattice sites occupied is determined by the radial temperature of the vertical lattice. Atoms load into  $\sim 100$  rows of tubes uniformly distributed along  $\hat{Y}$ , while the columns distributed along  $\hat{X}$  are loaded according to a Gaussian distribution with standard deviation  $\sigma_H$  of 6-10  $\mu\text{m}$ . After forming the lattices, we perform Doppler and sideband cooling using the  $^1S_0 - ^3P_1$ ,  $F = 11/2$  transition. Simultaneously, atoms are optically pumped to the  $m_I = +9/2$  ground state magnetic sublevel, using  $\sigma^+$ -polarized light on the  $^1S_0 - ^3P_1$ ,  $F = 9/2$  transition, propagating along a bias magnetic field parallel to  $\hat{Z}$ . We perform spectroscopy of the  $^1S_0 - ^3P_0$  transition using a narrow linewidth laser propagating along  $\hat{Y}$ .

We quantify the number of atoms by detecting fluorescence

on the strong  $^1S_0 - ^1P_1$  transition at 461 nm. Temperature information and trap frequencies are extracted from Doppler spectroscopy along  $\hat{Z}$  and vibrational sideband spectra [1, 14]. We estimate that we loaded  $\sim 7000$  atoms in the 1D lattice distributed in  $\sim 420$  pancakes and  $\sim 17$  atoms per pancake. We determine  $\omega_Y = 2\pi \times 80\ \text{kHz}$  and  $\omega_{X,Z} = 2\pi \times 500\ \text{Hz}$ , and  $T_{X,Y,Z} \sim 4\ \mu\text{K}$ . For the 2D lattice, we loaded  $\sim 3000$  atoms and estimate that 30% of the populated tubes are doubly occupied. We determine  $\omega_X = 2\pi \times 110\ \text{kHz}$ ,  $\omega_Y = 2\pi \times 70\ \text{kHz}$  and  $\omega_Z = 2\pi \times 800\ \text{Hz}$  at trap center, and  $T_{X,Y,Z} \sim 4.5\ \mu\text{K}$ .

ISB develop in the lineshape only in the parameter regime where  $\gamma \equiv E_{\text{int}}/\langle\tilde{\Omega}\rangle_T \gg 1$ . Here,  $E_{\text{int}} = (N-1)|\langle U\rangle_T|/2$  is the mean interaction energy per particle and  $N$  represents the number of atoms per lattice site.  $\langle U\rangle_T$  characterize the strength of two-body interactions and depends both on the confinement volume and temperature as [17]:  $\langle U\rangle_T \approx u\vartheta(\frac{\hbar\omega_X}{k_B T_X})\vartheta(\frac{\hbar\omega_Y}{k_B T_Y})\tilde{\vartheta}(\frac{\hbar\omega_Z}{k_B T_Z})$  with  $u = 4a_{eg}^- \sqrt{\frac{m\omega_X\omega_Y\omega_Z}{\hbar}}$ ,  $a_{eg}^-$  the singlet  $^1S_0 - ^3P_0$  scattering length [6] and  $\vartheta$  and  $\tilde{\vartheta}$  functions characterizing the temperature dependence, i.e.  $\vartheta(x \gg 1) \sim 2\tilde{\vartheta}(x \gg 1) \rightarrow 1$  and  $\vartheta(x \ll 1) \sim \tilde{\vartheta}(x \ll 1) \rightarrow \sqrt{x}$ . We used  $\langle O\rangle_T$  to denote the thermal average of  $O$ . In our experiment, the  $^1S_0 - ^3P_0$  spectroscopy is generally performed by using a 80-ms pulse and the ‘‘ $\pi$ -pulse’’ laser intensity is set to achieve maximum excitation fraction. We estimate  $\langle\tilde{\Omega}\rangle_T \sim 2\pi \times 6.25\ \text{Hz}$ .

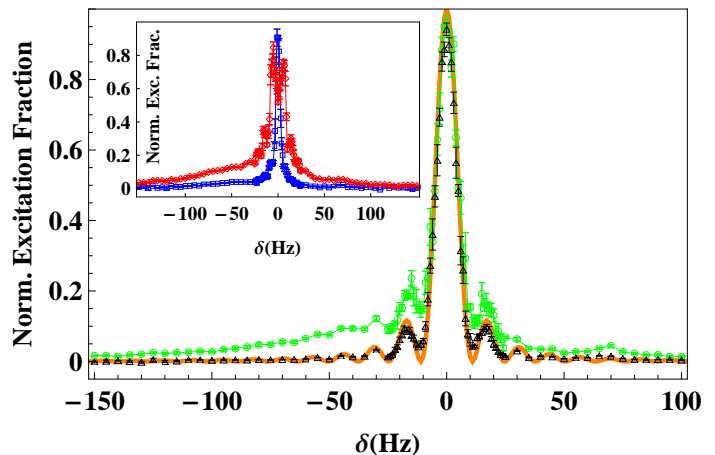


FIG. 2: (Color online) Measured Rabi lineshapes for  $g$  to  $e$  interrogation (normalized with respect to peak height). The main Panel shows lineshapes taken in a 1D lattice (black triangles) and in a 2D lattice (connected green circles) when the transition is excited with a  $\pi$ -pulse with 80 ms duration. The noninteracting, homogeneous Rabi lineshape for an 80 ms  $\pi$ -pulse is also shown (orange line). The inset shows lineshapes measured in a 2D lattice using a 160 ms  $2\pi$ -pulse (connected red diamonds) and a 160 ms  $\pi$ -pulse (connected blue squares). Each lineshape was measured under the trapping and temperature conditions described in the main text. The data from each lineshape is collected into bins 1-5 Hz wide.

Using the experimental trapping conditions and tempera-

tures and assuming a moderate  $a_{eg}^- = -70a_0$  ( $a_0$  the Bohr radius), we obtain  $\gamma^{2D} \sim 10$  in the doubly occupied sites at the center of the 2D lattice. On the contrary, for the central pancake of the 1D lattice with a mean number of 17 atoms and the same scattering length,  $\gamma$  is reduced to  $\gamma^{1D} \sim 0.6$ . Based on these values, one predicts the development of ISB only in the 2D lattice geometry, a prediction confirmed by our measurements. We measured a series of lineshapes in the 1D and 2D lattices. In the 2D lattice case we also varied the pulse area and Rabi frequency. The resulting data are shown in Fig. 2. To remove some of the statistical noise we performed multiple scans across the transition resonance under each experimental condition. For each scan, the drift of our ultra stable laser was canceled to  $<50$  mHz per second, and the laser was stepped by 2 Hz each experimental cycle ( $\sim 1.5$  sec). The center of each scan was determined by a fit to a Lorentzian. Each data set consists of  $\sim 20$  concatenated scans and the direction of the scan was alternated to reduce systematic effects due to residual drift. We separated the data into bins and calculated the mean and standard error of the mean for each bin. At our  $4 - 5$   $\mu\text{K}$  temperatures, the ISB in the 2D lattice are noticeable but nevertheless broad. To improve resolution, we reflect the binned lineshape at positive detuning (free of ISB when  $a_{eg}^- < 0$ ) and subtract it from the corresponding bin at negative detuning. The resultant lineshapes with a cleaner ISB are shown in Fig. 4.

The presence of ISB in the tightly confined geometry can be understood quantitatively by considering an isolated tube with  $N$  atoms. We characterize the tube dynamics by defining a set of effective spin operators,  $S_{n_j}^{x,y,z}$ , in the  $\{e, g\}$  basis [1, 11]. Here the subscript  $n_j$  is drawn from a fixed set  $\vec{n} = \{n_1, n_2 \dots n_N\}$  of initially populated vibrational modes along  $\hat{Z}$ . The description of the system in terms of effective spin operators is valid provided those initially populated modes remain singly occupied by either a  $g$  or an  $e$  atom during the excitation process. In the rotating frame, the Hamiltonian of the system up to constant terms becomes [11],

$$\frac{\hat{H}_{\vec{n}}^S}{\hbar} = -\delta S^z - \sum_{j=1}^N \Omega_{n_j} S_{n_j}^x - \sum_{j' \neq j}^N \frac{U_{n_j, n_{j'}}}{2} (\vec{S}_{n_j} \cdot \vec{S}_{n_{j'}} - \frac{1}{4}). \quad (1)$$

$S_j^{z,x}$  =  $\sum_{j=1}^N S_{n_j}^{z,x}$  are collective spin operators. The quantity  $U_{n_j, n_{j'}} = w \vartheta(\frac{\hbar \omega_X}{k_B T_X}) \vartheta(\frac{\hbar \omega_Y}{k_B T_Y}) I_{n_j, n_{j'}}$  measures the strength of the interactions between two atoms in the antisymmetric electronic state.  $I_{n_j, n_{j'}}$  is an overlap integral between harmonic oscillator modes along  $\hat{Z}$  [17]. Only the  $\hat{Z}$ -mode distribution is treated exactly since at current temperatures only a few transverse excited modes are populated. The population of transverse modes is accounted for as a renormalization of the interaction parameter.

The interaction part of the Hamiltonian is diagonal in the collective spin basis  $|S, M\rangle$ ,  $S = 0(\frac{1}{2}), \dots, N/2$  and  $|M| \leq S$ . For  $N = 2$ , the spin basis is spanned by the triplet states  $|1, M\rangle$  and the singlet  $|0, 0\rangle$ . Among the collective states only the  $S = N/2$  states are noninteracting. States with  $S < N/2$

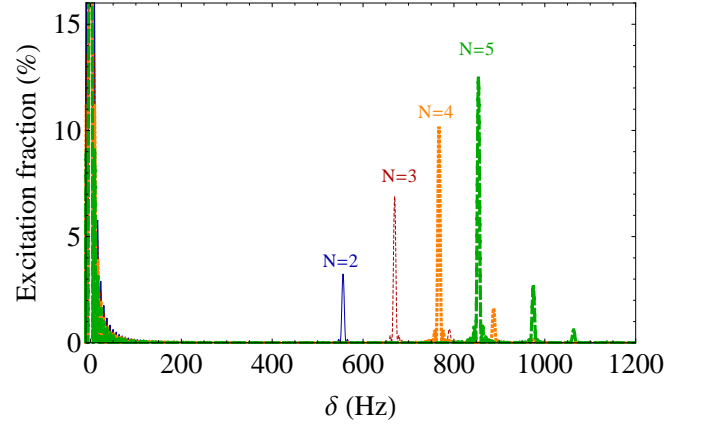


FIG. 3: (Color online) Excitation fraction vs.  $\delta$  at  $T = 0$  for lattice sites with  $N = 2 - 5$  atoms. The ISB reveal the  $S = N/2 - 1$  spectrum and can be used to probe occupation number in a lattice. The parameters used for the plot were  $\eta_Z = 0.4$ ,  $\Omega^B = 2\pi \times 5$  Hz,  $t = 1.5\pi/\Omega^B$  and  $u = 2\pi \times 2800$  Hz.

experience a finite interaction energy. In the presence of excitation inhomogeneity,  $S$  is no longer conserved and during excitation of the clock transition, atoms can be transferred mainly between  $S = N/2$  and  $S = N/2 - 1$  states. The  $N - 1$  collective excitation modes  $|S = N/2 - 1, M = N/2 - 1, q\rangle$  ( $q = 1, \dots, N - 1$ ) with energies  $U_{\vec{n}}^{q,N}$  can be accessed from the initially  $g$ -polarized state  $|N/2, -N/2\rangle$  using  $\delta \sim U_{\vec{n}}^{q,N}$ . They give rise to  $N - 1$  sidebands in the lineshape (Fig. 3):

$$N_{\vec{n}}^e(t, \delta) \approx N f(t, \delta, \bar{\Omega}_{\vec{n}}) + \sum_{q=1}^{N-1} f(t, \delta - U_{\vec{n}}^{q,N}, \Delta\Omega_{\vec{n}}^{q,N}) \quad (2)$$

with  $f(t, \delta, y) \equiv \frac{y^2}{y^2 + \delta^2} \sin^2\left(\frac{t\sqrt{y^2 + \delta^2}}{2}\right)$  and  $\Delta\Omega_{\vec{n}}^{q,N} = 2 \sum_j \Omega_{n_j} \langle N/2, N/2 | S_j^x | N/2 - 1, N/2 - 1, q \rangle$ . The first term is associated with the carrier and the second with the ISB. For the case  $N = 2$ , we have  $U_{\vec{n}}^{1,2} = U_{\vec{n}}$  and  $\Delta\Omega_{\vec{n}}^{1,2} = \Delta\Omega_{\vec{n}}$ .

At quantum degeneracy, only the lowest lying vibrational modes need to be considered  $\vec{n} = \{0, 1, \dots, N - 1\}$ . In this case, the interaction sidebands are very narrow. Assuming  $t = s\pi/\Omega^B$ , with  $s$  a numerical constant that describes the pulse duration, the peak width is just  $2\Omega^B/s$ . Measuring the interaction sidebands thus precisely determines  $a_{eg}^-$  and characterizes the  $S = N/2 - 1$  spectrum, which has structure for  $N > 2$ . Since the peak height of the interaction sidebands scales as  $\eta_Z^4$ , large probe inhomogeneities are required to observe them at low temperature.

In Ref. [9], interaction-dependent transition frequency shifts in RF spectroscopy were used to spectroscopically distinguish sites with different occupation numbers, revealing the shell structure of the Mott insulator phase. The  $g$  and  $e$  states in AEA have no hyperfine structure, and hence RF spectroscopy is not applicable. However, as shown in Fig. 3, the optical analog of RF spectroscopy—the ISB spectroscopy—can distinguish sites with different atom numbers. This ca-

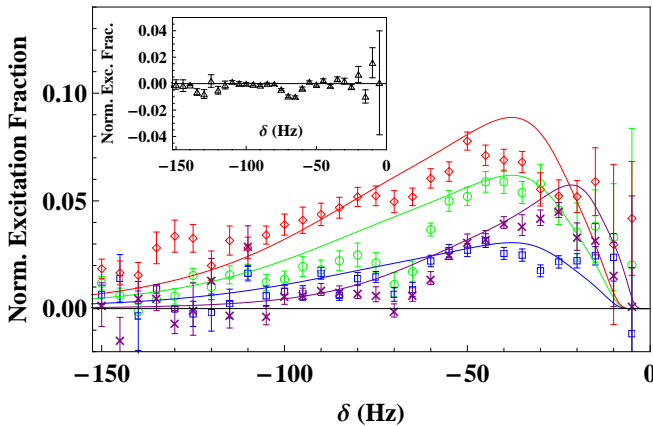


FIG. 4: (Color online) Finite temperature ISB in a 2D lattice ( $g$  to  $e$ ): Symbols correspond to experimental data obtained after reflecting the binned lineshape at positive detuning (free of ISB) and subtracting it from the corresponding bin at negative detuning. Data conditions previously shown in Fig. 2 are displayed with the same symbols and colors. The data indicated by purple crosses corresponds to an 80 ms  $\pi$ -pulse but with different trapping conditions ( $\omega_{X,Y,Z} = 2\pi \times \{92, 60, 0.6\}$  kHz at trap center,  $T_{X,Y,Z} \sim \{2.5, 2.5, 7.2\}$   $\mu$ K). The inset shows the absence of ISB in a 1D lattice. Solid curves correspond to theoretical predictions. The dip at  $\delta \sim -70$  Hz in the measured ISB is due to residual  $m_I = 7/2$  atoms.

pability can have important implications in quantum simulation [6] and information proposals [4] with AEA.

At finite  $T$ , instead of a fixed set of populated modes, a thermal average should be taken. For simplicity and to correspond to our current experiment, we focus on the  $N = 2$  case. After evaluating the thermal average [17], we obtain the following approximate expression for the ISB, valid in the regime  $|\delta| \gg \Omega^B$ ,  $k_B T_Z > \hbar\omega_Z$  and  $t = s\pi/\Omega^B \ll \langle \Delta\Omega \rangle_{T_Z}^{-1}$  (These conditions are satisfied in our experiment):

$$\langle \hat{N}^e \rangle_T \approx \frac{\eta_Z^4 \pi^2 \sqrt{\pi} s \Omega^B}{2 |\langle U \rangle_T|} \left( \frac{\hbar\omega_Z}{k_B T_Z} \right)^{-2} \left( \frac{\langle U \rangle_T}{\sqrt{\pi}\delta} \right)^7 e^{-\left(\frac{\langle U \rangle_T}{\sqrt{\pi}\delta}\right)^2}. \quad (3)$$

Fig. 4 shows comparisons between the measured ISB and theoretical curves calculated using Eq. (3). In the 2D lattice, sites near the wings of the lattice beams' Gaussian intensity profiles are significantly shallower than near the center of the beam intersection region, i.e.  $\omega_{\perp}(X, Y) \approx \omega_{\perp}(0, 0) \text{Exp}[-(X^2 + Y^2)/W_{\perp}^2]$ , with  $\omega_{\perp} \equiv \sqrt{\omega_X \omega_Y}$  and  $W_{\perp} \equiv \sqrt{W_X W_Y} \sim 30 \mu\text{m}$  the mean beam waist. This implies  $u$  varies from tube to tube; so to compare with experiment, it is important to average Eq. (3) over the populated tube distribution. We assume a uniform distribution of doubly occupied tubes. With this procedure, we obtain lineshapes that reproduce the experimental data if we use  $a_{eg}^- = -280a_0$  and  $\eta_Z \sim 0.07(0.05)$  for the  $\omega_{\perp} = 2\pi \times 87(73)$  kHz cases. The value of  $a_{eg}^-$  that fits the experimental data is outside the range of effective scattering lengths  $a_{eg}^* \sim -(35 - 50)a_0$  reported in Ref. [1]. However the discrepancy is attributed to the fact that  $a_{eg}^*$  in Ref. [1] corresponded to the effective scat-

tering length required to model the entire lattice array by a single tube at the trap center, and thus  $|a_{eg}^*|$  should be smaller than  $|a_{eg}^-|$ . In agreement with theory, the ISB's position and width are on the order of  $\langle U \rangle_T$  and their resonant peak heights (normalized to the carrier) decrease with decreasing  $\Omega^B$  and increase with pulse area  $s\pi$ .

We determine the nuclear spin purity of the atomic sample to be  $> 97\%$  by scanning the probe laser over the clock transition frequencies for other nuclear spin states. The signature of the remaining 3% is the small resonant peak at  $\delta \sim 70$  Hz in Fig. 2. By comparing the amplitude of this small peak with the ISB, we conclude that the observed sidebands are not caused by  $s$ -wave collisions between unpolarized atoms.

We also performed  $e$  to  $g$  Rabi interrogation by first transferring all the atoms from  $g$  to  $e$  with a resonant pulse, then removing the remaining  $g$  atoms and finally interrogating the  $e$  atoms with an 80 ms  $\pi$ -pulse. However, even in the tight geometry we did not see evidence of ISB in this case. The lack of ISB can be attributed to the absence of double occupancy in a single tube, possibly due to a combination of the following reasons. (1) A decrease in the number of interrogated atoms due to the additional steps required to prepare the atoms in  $e$ , (2) A more favorable transfer from  $g$  to  $e$  in tubes with a single atom and (3) Inelastic two-body  $e - e$  losses due to  $p$ -wave collisions similar to the ones recently measured in KRb molecules [15] and in  $^{88}\text{Sr}$  ( $s$ -wave) [16]. We measured the  $e$  atom lifetime in a 1D lattice to be 600ms. The measured loss rate, rescaled by the corresponding density in the tight confinement case, translates to decay rates about 30 times faster, i.e. lifetimes  $\sim 20$  ms. Given that there is a 10 ms waiting time between the preparation and the clock interrogation,  $e - e$  losses seem to be the relevant mechanism that leads to the absence of ISB.

The effect of tunneling between tubes could in principle modify the shape and height of the ISB (but not its mean position) and generate an additional frequency shift of the carrier. The latter can be particularly relevant in the strongly interacting regime where collisional shifts would otherwise be suppressed. In order to investigate the effect of tunneling, we also took one set of data under conditions which reproduced those used in Ref. [1]. The presence of ISB in this lineshape, measured with  $T_{X,Y} \sim 2.5 \mu\text{K}$  (see Fig. 4), completely rules out the possibility that these spectroscopic features are caused by tunneling since, under these conditions, we predict that tunneling rates are suppressed by two orders of magnitude compared to  $T_{X,Y} \sim 4.5 \mu\text{K}$ .

The studies presented here demonstrate that tools developed for clock experiments can provide precise understanding of strongly interacting many-body systems. This work was supported by ARO DARPA OLE, NIST, NSF, AFOSR, NRC, and Lee A. DuBridge and NDSEG fellowships.

- 
- [1] M. D. Swallows *et al.*, *Science* **331**, 1043 (2011); G. K. Campbell *et al.*, *Science* **324**, 360 (2009).
  - [2] N. D. Lemke *et al.*, *Phys. Rev. Lett.* **103**, 063001 (2009); A. D. Ludlow *et al.*, *Science* **319**, 1805 (2008); T. Akatsuka, M. Takamoto and H. Katori, *Nat. Phys.* **4**, 954 (2008); G. K. Campbell *et al.*, *Metrologia* **45**, 539-548 (2008); J. Ye, H. J. Kimble and H. Katori, *Science* **320**, 1734 (2008); A. D. Ludlow *et al.*, *Opt. Lett.* **32**, 641 (2007); M. M. Boyd *et al.*, *Phys. Rev. Lett.* **98**, 083002 (2007).
  - [3] C. W. Chou *et al.*, *Science* **329**, 1630 (2010).
  - [4] D. Hayes, P. S. Julienne, and I. H. Deutsch, *Phys. Rev. Lett.* **98**, 070501 (2007); A. J. Daley *et al.*, *Phys. Rev. Lett.* **101**, 170504 (2008); A. V. Gorshkov *et al.*, *Phys. Rev. Lett.* **102**, 110503 (2009); I. Reichenbach, P. S. Julienne, and I. H. Deutsch, *Phys. Rev. A* **80**, 020701 (2009).
  - [5] B. J. DeSalvo *et al.*, *Phys. Rev. Lett.* **105**, 030402 (2010); M. K. Tey *et al.*, *Phys. Rev. A* **82**, 011608 (2010); S. Taie *et al.*, *Phys. Rev. Lett.* **105**, 190401 (2010).
  - [6] A. V. Gorshkov *et al.*, *Nature Physics* **6**, 289 (2010); M. A. Cazalilla, A. F. Ho, and M. Ueda, *New J. Phys.* **11**, 103033 (2009); M. Hermele, V. Gurarie, and A. M. Rey, *Phys. Rev. Lett.* **103**, 135301 (2009); M. Foss-Feig, M. Hermele, and A. M. Rey, *Phys. Rev. A* **81**, 051603(R) (2010); M. Foss-Feig *et al.*, *Phys. Rev. A* **82**, 053624 (2010).
  - [7] T. C. Killian *et al.*, *Phys. Rev. Lett.* **81**, 3807 (1998).
  - [8] S. Giorgini, L. P. Pitaevskii and S. Stringari, *Rev. Mod. Phys.* **80**, 1215 (2008).
  - [9] G. K. Campbell *et al.*, *Science* **331**, 369 (2006).
  - [10] K. Gibble, *Phys. Rev. Lett.* **103**, 113202 (2009).
  - [11] A. M. Rey, A. V. Gorshkov, and C. Rubbo, *Phys. Rev. Lett.* **103**, 260402 (2009).
  - [12] D. J. Wineland and W. M. Itano, *Phys. Rev. A* **20**, 1521 (1979).
  - [13] H. Häffner *et al.*, *Phys. Rev. Lett.* **90**, 143602 (2003).
  - [14] S. Blatt *et al.*, *Phys. Rev. A* **80**, 052703 (2009).
  - [15] S. Ospelkaus *et al.*, *Science* **327**, 853 (2010).
  - [16] Ch. Lisdat *et al.*, *Phys. Rev. Lett.* **103**, 090801 (2009).
  - [17] See supplementary information.

## Supplemental material

### Interaction parameters

We consider nuclear-spin polarized fermionic atoms with two different electronic degrees of freedom ( $e, g$ ) confined in a harmonic trap with trapping frequencies  $\omega_{X,Y,Z}$  and assume the atoms interact only via s-wave interactions. The matrix element that describes collisions between two atoms ( $i = 1, 2$ ) in the  $\mathbf{n}_i = (n_{iX}, n_{iY}, n_{iZ})$  harmonic oscillator eigenmodes  $\phi_{n_{iX}}^X(X)\phi_{n_{iY}}^Y(Y)\phi_{n_{iZ}}^Z(Z)$  is given by

$$\begin{aligned} U_{\mathbf{n}_1, \mathbf{n}_2} &= \frac{8\pi\hbar a_{eg}^-}{m} \int d^3\mathbf{R} \prod_{\mu=X,Y,Z} [\phi_{n_{1\mu}}^\mu(\mu)]^2 [\phi_{n_{2\mu}}^\mu(\mu)]^2 \\ &= u I_{n_{1X}, n_{2X}} I_{n_{1Y}, n_{2Y}} I_{n_{1Z}, n_{2Z}}, \end{aligned} \quad (\text{A.4})$$

where  $\mathbf{R} = (X, Y, Z)$ ,  $u = 4a_{eg}^- \sqrt{\frac{m\omega_X\omega_Y\omega_Z}{h}}$ ,  $I_{n_1, n_2} = \frac{\sqrt{2} \int e^{-2z^2} H_{n_1}^2(z) H_{n_2}^2(z) dz}{\sqrt{\pi} 2^{n_1+n_2} (n_1!)(n_2!)}$ , and  $H_n(z)$  are Hermite polynomials.

At finite temperature, expectation values need to be calculated by averaging over all possible combinations of modes weighted according to their Boltzmann factor:  $\langle U \rangle_T \approx u \vartheta(\frac{\hbar\omega_X}{k_B T_X}) \vartheta(\frac{\hbar\omega_Y}{k_B T_Y}) \tilde{\vartheta}(\frac{\hbar\omega_Z}{k_B T_Z})$  with  $\vartheta(\alpha) \equiv \frac{\sum_{n_1, n_2} I_{n_1, n_2} e^{-\alpha(n_1+n_2)}}{\sum_{n_1, n_2} e^{-\alpha(n_1+n_2)}}$  and  $\tilde{\vartheta}(\alpha) \equiv \frac{\sum_{n_1 > n_2} I_{n_1, n_2} e^{-\alpha(n_1+n_2)}}{\sum_{n_1 > n_2} e^{-\alpha(n_1+n_2)}}$ . The  $\tilde{\vartheta}$  function is introduced since in our experiment atoms start polarized in  $g$ , and even at  $T = 0$  they are required to occupy different modes along  $\hat{Z}$  to satisfy the Pauli exclusion principle.

For  $\frac{\hbar\omega_Z}{k_B T_Z} \ll 1$ , eigenmodes with  $|n_{1Z} - n_{2Z}| \gg 1$  dominate, so that

$$I_{n_{1Z}, n_{2Z}} \approx 2 \frac{K \left[ \frac{1}{2} \left( 1 - \frac{n_{1Z} + n_{2Z}}{|n_{1Z} - n_{2Z}|} \right) \right]}{\pi \sqrt{\pi |n_{1Z} - n_{2Z}|}}, \quad (\text{A.5})$$

where  $K$  is the complete elliptic integral of the first kind. Furthermore, we checked numerically that, for our parameters, ISB is not significantly perturbed by approximating  $K$  with  $K(0)$ , so that  $I_{n_{1Z}, n_{2Z}} \approx \frac{1}{\sqrt{\pi} \sqrt{|n_{1Z} - n_{2Z}|}}$ . Using this approximation, one can show that  $\vartheta(\alpha \ll 1) \sim \tilde{\vartheta}(\alpha \ll 1) \sim \sqrt{\alpha}$ .

The (absolute value of the) mean interaction energy per particle  $E_{\text{int}}$  is  $(N-1)|\langle U \rangle_T|/2$ , where  $N$  is the number of atoms in the trap.

### Interaction sidebands (ISB) at finite Temperature for two atoms (N=2)

Here, we derive Eq. (3) in the main text by performing a thermal average over different axial modes. First, consider a given set of populated modes along  $\hat{Z}$ ,  $\vec{n} = (n_1, n_2)$ . If the atoms are in the strongly interacting regime,  $|U_{\vec{n}}| \gg \Omega_{\vec{n}}$ , the ISB is given by

$$N_{\vec{n}}^e(t, \delta) \approx f(t, \delta - U_{\vec{n}}, \Delta\Omega_{\vec{n}}) \quad (\text{A.6})$$

with  $f(t, \delta, y) \equiv \frac{y^2}{y^2 + \delta^2} \sin^2 \left( \frac{t\sqrt{y^2 + \delta^2}}{2} \right)$ .

At finite temperature, we need to evaluate  $\langle N^e \rangle_T = \frac{\sum_{n_1 > n_2} N_{\vec{n}}^e(t, \delta) e^{-\alpha(n_1+n_2)}}{\sum_{n_1 > n_2} e^{-\alpha(n_1+n_2)}}$  with  $\alpha = \frac{\hbar\omega_Z}{k_B T_Z}$ . We evaluate  $\langle N^e \rangle_T$  under the approximations  $\Delta\Omega_{\vec{n}} \approx \frac{\Omega_B \eta_Z^2 (n_1 - n_2)}{\sqrt{2}}$  and  $U_{\vec{n}} \approx \vartheta(\frac{\hbar\omega_X}{k_B T_X}) \vartheta(\frac{\hbar\omega_Y}{k_B T_Y}) \frac{u}{\sqrt{\pi |n_1 - n_2|}} \equiv \frac{\xi}{\sqrt{\alpha |n_1 - n_2|}}$ .

To carry out the sum, we treat  $\alpha(n_1 - n_2) \equiv x$  and  $\alpha(n_1 + n_2) \equiv y$  as continuous variables (valid if  $\alpha \ll 1$ ). We also define  $\kappa(x) = \frac{\Omega_B \eta_Z^2 x}{\alpha \sqrt{2}} \equiv bx$  and  $U(x) = \frac{\xi}{\sqrt{x}}$ . Then  $\langle N^e \rangle_T \approx \int_0^\infty N^e(x/\alpha) e^{-x} dx$  with  $N^e(x/\alpha) = \frac{\kappa^2(x)}{\kappa^2(x)^2 + \delta^2} \sin^2 \left( \frac{t\sqrt{\kappa^2(x) + (\delta - U(x))^2}}{2} \right)$ . Noticing that  $N^e$  is sharply peaked at  $x_0 = (\xi/\delta)^2$ , we evaluate  $e^{-x}$  and  $\kappa$  at  $x = x_0$ . We write  $x = x_0 + x'$  and expand  $U$  in  $x'$  to first order. We then define  $p = |\xi|x'/(2bx_0^{5/2})$ , so that

$$\begin{aligned} \langle N^e \rangle_T &\approx e^{-x_0} \frac{2bx_0^{5/2}}{|\xi|} \times \\ &\int_{-\infty}^{\infty} dp \frac{1}{1+p^2} \sin^2 \left( c\sqrt{1+p^2} \right), \end{aligned} \quad (\text{A.7})$$

where  $c = tbx_0/2$ . For  $c \ll 1$ , the integral in Eq. (S4) is approximately equal to  $\pi c$ . This yields Eq. (3) in the main text.